



HAL
open science

Redox properties of the carbonate molten salt

$\text{Li}_2\text{CO}_3\text{Na}_2\text{CO}_3\text{-K}_2\text{CO}_3$

Hugo Sauzet, Romaric Collet, Christophe Héau, Christophe Pupier, Davide Rodrigues, Céline Cannes, Sylvie Delpech

► **To cite this version:**

Hugo Sauzet, Romaric Collet, Christophe Héau, Christophe Pupier, Davide Rodrigues, et al.. Redox properties of the carbonate molten salt $\text{Li}_2\text{CO}_3\text{Na}_2\text{CO}_3\text{-K}_2\text{CO}_3$. *Electrochimica Acta*, 2022, 405, pp.139765. 10.1016/j.electacta.2021.139765 . hal-03578840

HAL Id: hal-03578840

<https://hal.science/hal-03578840v1>

Submitted on 12 Oct 2022

HAL is a multi-disciplinary open access archive for the deposit and dissemination of scientific research documents, whether they are published or not. The documents may come from teaching and research institutions in France or abroad, or from public or private research centers.

L'archive ouverte pluridisciplinaire **HAL**, est destinée au dépôt et à la diffusion de documents scientifiques de niveau recherche, publiés ou non, émanant des établissements d'enseignement et de recherche français ou étrangers, des laboratoires publics ou privés.

Redox properties of the carbonate molten salt $\text{Li}_2\text{CO}_3\text{-Na}_2\text{CO}_3\text{-K}_2\text{CO}_3$

Hugo Sauzet^{1,2}, Romaric Collet², Christophe Héau², Christophe Pupier², Davide Rodrigues¹, Céline Cannes¹, Sylvie Delpech¹

1 Université Paris-Saclay, CNRS/IN2P3, IJCLab, 91405 Orsay, France

2 IREIS, HEF Groupe, ZI Sud – 69 Avenue Benoît Fourneyron, CS 42077-42162 Andrézieux-Bouthéon, France

Abstract

The objective of this work is to study the $\text{Li}_2\text{CO}_3\text{-Na}_2\text{CO}_3\text{-K}_2\text{CO}_3$ (29.5-31.1-39.4 mol%) molten salt and the behaviour of several metals (Au, Pt, C, Ni and W) by electrochemical measurements in the salt under three atmospheres (Ar, CO_2 and O_2/N_2). Thermodynamic calculations show that the molten salt anodic and cathodic limits correspond to the carbonate ions oxidation and reduction to dioxygen and carbon respectively. An internal reference electrode has been defined based on the redox system $\text{Na}^+/\text{Au}_2\text{Na}$, which is independent of the lithium oxide activity.

The widths of the electroactivity domain have been measured on gold working electrode by cyclic voltammetry: 2.21 V under Ar and O_2/N_2 and 2.41 V under CO_2 , which are larger than the values obtained by thermodynamic calculations (1.280 V and 1.025 V respectively). Gas chromatographic (GC) analysis during electrolysis at potentials ranging in the anodic limit allowed to conclude that the electrochemical domain of the carbonate molten salt is limited anodically by the oxidation of carbonate ions to dioxygen, possibly peroxide ions, and carbon dioxide. The characterisation by XRD of a platinum electrode after electrolysis at the cathodic limit has shown that the electroactivity domain of the molten salt is defined by the carbonate ions reduction into carbon, indicating that $\text{CO}_3^{2-}/\text{C}$ is an irreversible system. A carbonate ions decomposition rate of $1 \times 10^{-3} \text{ mmol.h}^{-1}.\text{cm}^{-2}$ has been determined by GC and thermogravimetric analysis (TGA) under inert gas. A stabilization of the CO_2 pressure is observed after the melting of the salt.

Keywords: $\text{Li}_2\text{CO}_3\text{-Na}_2\text{CO}_3\text{-K}_2\text{CO}_3$; Carbonates; Electrochemistry; Gas chromatography; thermodynamic calculation; Au_2Na alloy; Molten salt.

1 Introduction

Alkali carbonate have been studied in the past for the development of the Molten Carbonate Fuel Cell (MCFC) energy supplier [1]–[4]. Carbonate molten salts can also be used for other applications. In order to decrease greenhouse effect, global emission must be reduced or carbon dioxide must be captured. Sugiura *et al.* tried to combine MCFC with thermal power plant to limit carbon dioxide emission [5]. Some other capture and storage devices are in development such as membranes composed of carbonate molten salt [6], [7]. Chery studied the CO_2 solubility in molten carbonate. The objective is to transform CO_2 into C or CO and reuse these products [8]. Carbonate molten salts can also be used for metals recycling. Yasuda *et al.* used sodium carbonate to dissolve and to recycle tungsten and tungsten carbide [9].

Thermodynamic, chemical and electrochemical properties of alkali carbonate molten salts have already been presented [10]–[13]. The different oxides forms were identified as oxide, peroxide and superoxide ions and their proportions were determined in several composition of lithium, sodium and potassium carbonate salts, by considering either the pure bodies or binary and ternary eutectics [10], [11]. The electrochemical domains of these carbonate salts were determined by calculating the potential of each redox couple as a function of the carbon dioxide partial pressure [8], [12], [13]. Chemical and electrochemical properties of the carbonate salts were also widely presented [7], [12], [14]–[16].

Carbonate salts are also used in nitriding molten salts. Nitriding salts are mainly used for the treatment of steels in order to increase their superficial hardness and wear resistance with the formation of iron nitride. These salts are composed of carbonate and cyanate ions [17]–[19]. The alkali carbonates represent the solvent and the cyanate ions, the reagent which decomposes spontaneously to produce nitrogen (that diffuses inside steel) and cyanide ions. For economic reason, the nitriding molten salts are richer in sodium and potassium carbonates than lithium ones.

Few electrochemical studies have been done in nitriding salt. So, the objective is to study the carbonate molten salt used as solvent for the nitriding processes. From the redox properties determined with this salt, it will be easier to work with a complete nitriding salt. Then, the salt study in this work does not contain cyanate ions. The composition of the selected salt for this study is $\text{Li}_2\text{CO}_3 - \text{Na}_2\text{CO}_3 - \text{K}_2\text{CO}_3$ (29.5 - 31.1 - 39.4 %mol). The composition of the ternary

eutectic of the alkali carbonate salts is different: Li_2CO_3 - Na_2CO_3 - K_2CO_3 (43.5 - 31.5 – 25 % mol). Thermodynamic studies of this ternary eutectic have already been presented at 550°C and 650°C by Moutiers[12]. But, as the working temperature and the salt composition are different, thermodynamic data have been calculated for the selected carbonate salts and at 600°C. The electrochemical domain has been determined from these thermodynamic calculations and has been compared to the one measured experimentally by combining electrochemical measurements (cyclic voltammetry and electrolysis), gas analysis by chromatography and characterisation by X ray diffractometry under different atmospheres. The materials of the working and auxiliary electrodes have been selected after determination of their stability domain in the carbonates salt by thermodynamic calculations. This work has also concerned the selection of the reference electrode for the electrochemical experiments. Finally, carbonates salt decomposition has been studied by thermogravimetric analysis (TGA) and gas chromatography.

2 Experimental section

2.1 Materials and chemical reagents

Chemical reagents and molten salt preparation

Lithium, sodium and potassium carbonates were provided by Sigma Aldrich reagents with high purity (>99.0%). Table 1 gives the composition of the ternary molten salt used in this study. The three carbonate salts (total mass: 100 g) were mixed inside a sintered alumina crucible (99.7% purity – Final Advanced Materials) and placed into a quartz cell hermetically closed and constituted of two parts, a top and a bottom one (Figure 1). The air tightness was maintained using a locking screw. The electrochemical cell was then introduced in a tubular furnace (80 mm diameter) connected to a regulation monitor provided by THERMOLAB/Spain. The mixture was melted by increasing the temperature to 873 K. The temperature was measured inside the molten salt by a thermocouple (Thermo Scientific) protected by an alumina sheath. The salt melting was performed under CO_2 atmosphere (except when the carbonate decomposition was studied). If any alkaline oxide impurities are inside the molten salt, CO_2 should react and transform oxide species into carbonate species. After 24 h, the chosen working atmosphere was introduced and a bubbling inside the molten salt was realized for 10 hours. Then the gas flow was maintained above the molten salt all along the measurements. The study was conducted under three gaseous atmospheres N_2/O_2 (80%/20%), Ar and CO_2 . The 3 gases were provided by Air Liquide, quality Alphagaz 1.

2.2 Thermodynamic calculations and experimental measurements

Thermodynamic calculations were performed to determine the redox potentials by using the database and software *HSC 6 Chemistry* database.

Electrochemical measurements were conducted with a Princetown Applied Research Potentiostat (model Versastat 3F) controlled by a personal computer (DELL OptiPlex 3020) and the software Versastudio. A three electrode-cell system was used for cyclic voltammetry and electrolysis in the salt (Figure 1).

Several electrode materials have been tested: gold (wire, 1 mm diameter, 99.95% purity), platinum (wire, 1 mm diameter, 99.95% purity), Ni (wire 1 mm diameter, 99.98% purity), silver (wire, 1 mm diameter, 99.99% purity) and tungsten (wire, 1 mm diameter, 99.95% purity). They were all provided by Goodfellow. For the reference electrode, three possible systems was addressed [20]: thermodynamic, internal and pseudo-reference electrode. Thermodynamic reference requires a permeable membrane: alumina (AL23 Degussit Ø5x8 >99.5% purity), mullite (C530 Umicore Ø6x10) and Pyrex (Techlab Ø4x6) were used [21].

Gas chromatography analyses were conducted with a Inficon MicroGC fusion which is equipped with two modules: Rt-Molsieve 5A (0.25 mm diameter and 10 m length) [RT-Q-Bond (3 m)] TCD2 for H₂, O₂, N₂ and CO analyses and RT-Q-Bond (0.25 mm diameter and 12 m length) TCD2 for CO₂ and H₂O analyses, controlled by a personal computer (Dell OptiPlex 5080). The software used was Micro GC Fusion Offline Analysis. Both modules were calibrated with a gas mixture provided by Air Product. The apparatus was placed after an empty guard to prevent water to go inside it (Figure 1).

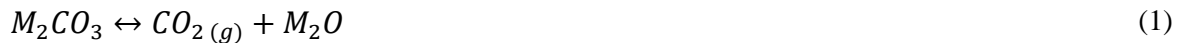
XRD analyses were conducted with a D8advance Bruker XRD with a $\lambda Cu_{K\alpha 1} = 1.5406 \text{ \AA}$ controlled by a personal computer (HP compaq) and the diffractometer were analysed using the software EVA.

Thermogravimetry Analyses were conducted with a Netzsch STA 449 F3 Jupiter TGA. 1500.953 mg of the salt (presented in the Table 1) was mixed in a sintered alumina crucible (Netzsch). The study was conducted under Ar atmosphere provided by Air Liquide, quality Alphagaz 1. The gas flow was 60 mL.min⁻¹. The temperature was increased from 298 K to 573 K with a temperature ramp of 5 K.min⁻¹. An isotherm of 8 h was imposed at 573 K in order to remove moisture. Then, the temperature was increased from 573 K to 873 K with a ramp of 5 K.min⁻¹. An isotherm of 70 h was imposed at 873 K to follow the carbonates decomposition. TGA was controlled by a personal computer (DELL PowerEdge T110) with Netzsch Proteus Thermal Analysis software.

3 Results and discussion

3.1 Thermodynamic calculations

The stability domain of a solvent and its solutes is usually described using potential-acidity diagrams. That is the case in aqueous solution with the Pourbaix diagrams in which the redox potential E is plotted vs pH [22]. Littlewood extended this approach to fused chlorides with similar plots of E vs pO^{2-} ($= -\log(O^{2-})$) [23]. Littlewood introduced the concept of oxoacidity where an oxobase species is able to release oxide ion (O^{2-}) whereas an oxoacid species can capture this oxide. Oxoacidity is presented by a logarithm scale of the oxide ion activity. This can be compared to the acidity scale given by the activity of H^+ ion in aqueous solution. Oxobasic systems are rich in oxide ions whereas oxoacid systems contain a small quantity of oxide ions. In carbonate molten salts, Ingram and Janz were the first to calculate these diagrams plotting E vs pCO_2 ($= -\log P(CO_2)$) [24]. The dissociation of the carbonate salt gives rise to the well-defined acid-base reaction (1) which is equivalent to the reaction (2) [14].



Therefore, the oxoacidity of the melt may be expressed either as $pa(M_2O)$ ($= -\log a(M_2O)$) where $a(i)$ is the activity of the species (i) or as pCO_2 . In this paper, the thermodynamic diagrams are presented by plotting E vs $pa(M_2O)$, where M corresponds to either Li, Na or K. The decomposition of the carbonate salt, the amount of O^{2-} and thus, the chemistry of the salt, is strongly governed by the nature of the gas in equilibrium with the salt. Several atmospheres have been studied in this paper: Ar, CO_2 and Air ($N_2/O_2 = 80/20\%$). *HSC 6 Chemistry* database was used for calculations.

3.1.1 Fused salt stability domain

Oxoacidity domain –The molten salt oxoacidity range is determined considering the autodissociation equilibrium (3) characterized by the constant K_Ω given by:

$$K_\Omega = \frac{a_{M_2O} \times P_{CO_2}}{a_{M_2CO_3}} \quad (3)$$

The oxobasic limit is defined by the saturation of the molten salt by M_2O which corresponds to a_{M_2O} equal to 1, whereas the oxoacidic limit is obtained for a partial pressure of carbon dioxide equal to 1 bar. Table 2 gives the constants calculated using *HSC 6.0* database for each

alkali carbonate. Since, lithium carbonate presents the highest autodissociation constant, the oxobasic limit corresponds to the precipitation of Li_2O .

The oxoacidic limit is defined by a carbon dioxide pressure of 1 bar. The corresponding value of $a_{\text{Li}_2\text{O}}$ is determined from relation (3). As no thermodynamic data are available for the ternary molten salt $\text{Li}_2\text{CO}_3\text{-Na}_2\text{CO}_3\text{-K}_2\text{CO}_3$, the salt is considered as an ideal mixture. Thus, in all the thermodynamic calculations $a_{\text{M}_2\text{CO}_3}$ is considered equal to its mole fraction $x_{\text{M}_2\text{CO}_3}$ in the molten salt (given in the Table 1). Table 3 presents the oxoacidity limits of the studied molten salt.

Electrochemical domain – The electroactivity domain is the potential range of stability of an electrolyte. It is limited by the anodic and cathodic limits of the electrolyte. These electrochemical limits are defined by the oxidation and the reduction of the components of the molten salt. The alkaline salts are considered totally dissociated to CO_3^{2-} , Li^+ , Na^+ and K^+ . Thus, the components which can be reduced are:

- Alkali ions into alkali metal as presented in reaction (4),
- Carbonate ions into carbon or carbon monoxide as presented in reactions (5) and (6) respectively.



With $M = \text{Li}, \text{Na}$ or K



The only components that can be oxidised is carbonate ions, to dioxygen (O_2 – reaction (7)), peroxide ions (O_2^{2-} - reaction (8)) or superoxide ions (O_2^- - reaction (9)).



For the thermodynamic calculations, it is necessary to fix a redox system as a reference electrode. In this study, the redox system $\text{Li}_2\text{CO}_3/\text{Li}$ is considered as the reference system. The redox reaction and the associated Nernst relation are given by relations (10) and (11).



$$E_{Li^+/Li} = E_{Li^+/Li}^0 + \frac{2.3RT}{nF} \log \frac{a_{Li_2CO_3}}{a_{Li}^2 \times a_{CO_3^{2-}}} \quad (11)$$

With $E_{Li^+/Li}^0 = 0 V$ (reference redox couple), $a_{Li_2CO_3} = x_{Li_2CO_3}$ and $a_{Li} = a_{CO_3^{2-}} = 1$ (Li is the metal and CO_3^{2-} is the only anion in the melt, its activity is considered equal to 1)

All the redox potentials are calculated against Li^+/Li (equivalent to Li_2CO_3/Li) redox system. As an example, for the oxidation of carbonate ion CO_3^{2-} to dioxygen O_2 (equation (12)), the redox potential is expressed by the Nernst relation (equation (13)).



$$E_{O_2/CO_3^{2-}} = E_{O_2/CO_3^{2-}}^0 + \frac{2.3RT}{nF} \log \frac{P_{O_2}^{0.5} \times P_{CO_2}}{a_{CO_3^{2-}}} \quad (13)$$

$$E_{O_2/CO_3^{2-}} = E_{O_2/CO_3^{2-}}^0 + \frac{2.3RT}{nF} \log(K_\Omega \times a_{Li_2CO_3}) + \frac{2.3RT}{nF} pa(Li_2O)$$

Where P_{O_2} , the partial pressure of O_2 , is considered equal to 1 for these calculations. $a_{CO_3^{2-}}$ is considered equal to 1. P_{CO_2} is related to a_{Li_2O} as seen in relation (3) and K_Ω is the dissociation constant of Li_2CO_3 .

The relation E - $pa(Li_2O)$ for the redox system O_2/CO_3^{2-} has been established. To be able to plot the diagram, the unknown parameter, $E_{O_2/CO_3^{2-}}^0$, has to be determined against the reference system considered.

The two half-reactions (10) and (12) lead to the chemical reaction (14) characterized by the equilibrium constant K_Φ and the enthalpy energy expressed by the relations (15) and (16).



$$K_\Phi = \left(\frac{a_{O_2}^{0.5} \times P_{CO_2} \times a_{Li}^2}{a_{Li_2CO_3}} \right) \quad (15)$$

$$\Delta G^\circ_\Phi = -2.3RT \log K_\Phi \quad (16)$$

At equilibrium, $E_{O_2/CO_3^{2-}} = E_{Li^+/Li}$. Then, from relations (11) and (13), the relation (17) is deduced.

$$E_{Li^+/Li}^0 + \frac{2.3RT}{nF} \log \frac{a_{Li_2CO_3}}{a_{Li}^2 \times a_{CO_3^{2-}}} = E_{O_2/CO_3^{2-}}^0 + \frac{2.3RT}{nF} \log \frac{a_{O_2}^{0.5} \times P_{CO_2}}{a_{CO_3^{2-}}} \quad (17)$$

From the relations (16) and (17), relation (18) is obtained.

$$\begin{aligned} E_{O_2/CO_3^{2-}}^0 &= E_{Li^+/Li}^0 + \frac{2.3RT}{nF} \log \frac{a_{Li_2CO_3}}{a_{Li}^2 \times a_{O_2}^{0.5} \times P_{CO_2}} \\ &= E_{Li^+/Li}^0 + \frac{2.3RT}{nF} \log \frac{1}{K_\Phi} = \frac{\Delta G^\circ_\Phi}{nF} \end{aligned} \quad (18)$$

Li^+/Li being the reference redox system, $E_{Li^+/Li}^0 = 0 V$.

Finally, the general relation E-pa(Li_2O) (relation (19)) is defined by combining the relations (13) and (18).

$$E_{O_2/CO_3^{2-}} = \frac{\Delta G^\circ_\Phi}{nF} + \frac{2.3RT}{nF} \log(K_\Omega \times a_{Li_2CO_3}) + \frac{2.3RT}{nF} pa(Li_2O) \quad (19)$$

Table 4 presents the redox couples and their associated $E = f(a_{Li_2O})$ relations. Using these relations, the stability domain of the ternary alkali carbonate fused salt has been constructed (Figure 2a). An anodic limit is observed and corresponds to carbonate ions oxidation into dioxygen. The cathodic limit corresponds to the carbonate ions reduction into carbon. The thermodynamic electro-activity domain is equal to 1.280 V under N_2/O_2 and Ar atmospheres and 1.025 V under CO_2 atmosphere. No stability domain of $CO(g)$ is observed. A previous diagram was calculated by Cassir *et al.* [13]. These authors have shown that the thermodynamic cathodic limit corresponds to the potassium ion reduction to potassium in oxobasic media and by the carbonate ions reduction to CO or C in oxoacid media. Furthermore, they have calculated that the anodic limit is defined by carbonate ions oxidation to peroxide and superoxide ions when these species activity are equal to 10^{-3} in oxobasic media. We did these calculations considering peroxide and superoxide at low concentrations and we obtain the diagram given Figure 2b which is similar to the one calculated by Cassir *et al.* The differences observed with the work of Cassir *et al.* for the cathodic limit can be explained by a composition of the salt different ($Li_2CO_3 - Na_2CO_3 - K_2CO_3$ (43.5 – 31.5 – 25 %mol) for Cassir *et al.* [13]) and by the evolution of the thermodynamic databases since 19XX.

3.1.2 Elements stability domain in fused alkali carbonate

Elements of interest – To conduct electrochemical studies in the molten alkali carbonate, the choice of the material electrodes has been based on a preliminary thermodynamic study of

different elements in order to determine their stability in the melt. Five materials are investigated: gold and platinum as working or counter electrode, and nickel, tungsten and carbon as pseudo-reference. Thermodynamic calculations are performed following the way presented previously. Table 5 gathers the redox systems considered and their associated $E = f(a_{Li_2O})$ relations.

Gold and platinum – For gold, the species Au, AuO and Au₂O₃ have been considered. Figure 3 presents the potential-acidity diagram of gold in molten carbonate at 873 K. It shows that gold is thermodynamically stable in the molten carbonate in all the range of potential and acidity. That is confirmed by the studies of Trémillon [14] and Ingram and Janz [24].

For platinum thermodynamic calculations, the species Pt, PtO, Pt₃O₄ and PtO₂ have been considered. Figure 3 presents the potential-acidity diagram of platinum in molten carbonate at 873 K. Platinum metal has a wide range of stability but the oxidation of Pt to PtO is close to carbonate oxidation into dioxygen. Ingram and Janz suggested from thermodynamic calculations that platinum should be immunised or passivated in carbonate ternary eutectic at 873 K [24]. Janz and Conte also suggested the possibility to have the oxide Li₂PtO₃ after platinum immersion inside the salt [25]. The thermochemical data relative to this oxide being not available in the used database, it was not possible to do the calculations for this compound.

Carbon, Nickel, Tungsten – Carbon stability diagram has been presented in the carbonate stability domain (Figure 2). This diagram shows that carbon should be stable in carbonate and be oxidised by dioxygen. For nickel thermodynamic calculations, the species Ni, NiO and NiCO₃ have been considered. Figure 4 presents potential-acidity diagram of nickel in molten carbonate at 873 K. Ni and NiO are the two stable species in the molten salt depending on the potential. Using other calculation parameters, Malinowska *et al.* have evidenced a stability domain for NiCO₃, NaNiO₂ and Na₂NiO₂ [26]. According to their calculations, NiCO₃ is stable in oxoacid salt. This calculation has been done for an activity of NiCO₃ equal to 10⁻⁵ whereas in this study, the NiCO₃ activity has been taken equal to 10⁻³. Malinowska *et al.* did not have thermodynamic data on lithium-nickel oxides but they supposed that such oxide should be more stable than NaNiO₂ and Na₂NiO₂ [26]. The *HSC Chemistry 6* thermodynamic database used in this study does not provide any data on lithium-nickel oxides nor sodium-nickel oxides.

The chemical forms W, WO, WO₂, WO₃, W₂O₆, W₃O₈, W₃O₉, W₄O₁₂, W₅O₁₅, Li₂WO₄, Na₂W₂O₇ and Na₂WO₄ have been considered for tungsten thermodynamic calculations. Figure 4 presents the potential-acidity diagram of tungsten in molten carbonate at 873 K. It shows that

tungsten is not stable in the carbonate salt. It is oxidised to Na_2WO_4 with formation of C. Yasuda *et al.* thermodynamic calculations in Na_2CO_3 molten salt at 1173 K led to the same result [9].

3.2 Electrodes materials selection for electrochemical measurements

Working electrode – According to the literatures, gold was mainly used as working electrode [12], [24], [25], [27]. Furthermore, our thermodynamic calculations show that gold is stable in carbonate molten salt. Thus, gold has been chosen as working electrode.

Counter electrode – In molten carbonate, different counter electrodes are used: gold wire [12] or graphite rod [28] [29]. Furthermore, our thermodynamic calculations show that platinum is immunised in the ternary salt. Platinum has then been selected as auxiliary electrode in this work.

Reference electrode – Thermodynamic, pseudo-reference and internal reference have been studied in molten carbonate salts.

Thermodynamic reference

Thermodynamic reference is based on a redox system isolated from the electrolyte by a membrane. In molten salts, the reference system is contained in a sheath that allows ionic conduction. Three thermodynamic references electrodes have been studied in this molten salt as described Figure 5.

Ag₂SO₄/Ag - Alumina sheath – This reference system has already been used in the ternary eutectic salt [12]. In this work, no electrochemical signal was obtained during experiments conducted with this electrode immersed in the salt. Generally, to allow ionic conduction, a silicoaluminous sintered part is added at the end of the sheath or a hole is performed in the bottom of the sheath. These two options cannot be retained because the risk of salt pollution is too high (break of the sintered part or diffusion of silver ions through the hole).

AgCl/Ag - Mullite sheath – Porous mullite (also known as Pythagoras porcelain) can also be used as the sheath for the reference electrode containing a Ag(I)/Ag redox couple [30] , [31]. A silver wire has been immersed in a LiCl-KCl salt containing AgCl (0.1 mol.kg^{-1}) and the sheath has been sealed with a silicone. Proper electrochemical results have been obtained the first 24 h. However, after 24 h, it became impossible to conduct electrochemical measurements. It is suspected that salt has come inside the sheath because of porous structure of mullite and a

crystallisation has occurred in the reference electrode sheath leading to the loss of ionic conduction.

NiF₂/Ni - Pyrex – Finally, a third reference electrode has been described by Duran-Klie [32]. It is composed by a Pyrex sheath and the redox couple Ni(II)/Ni. A Nickel wire is immersed inside the LiF-NaF-KF eutectic containing NiF₂ (10⁻² mol.kg⁻¹). The sheath is then sealed with silicone. Figure 6 presents cyclic voltammograms realized at a gold electrode in the Li₂CO₃-Na₂CO₃-K₂CO₃ melt at 873 K with this reference electrode. Even if electrochemical measurements can be conducted, Pyrex is not stable and is dissolved in the molten carbonate contributing to a salt pollution. After 12 days of immersion, silicon concentration has been measured by ICP-AES and determined to be 531 mg/kg. When high concentration of silicon is attained in the salt, a coating on side gold and platinum electrodes is observed: XRD analyses demonstrate the deposition of NaLi₃SiO₄ on electrodes surface. Formation of this species can be explained by carbonate and silicate reaction as given in relation (20). Moreover, after more than 7 days of immersion, the Pyrex sheath is likely to break. Generally, when this type of electrode is used in the molten salt, the reference has to be replaced every week.



$$\Delta G_{873 K}^0 = -39,961 kJ/mol \text{ of } SiO_2$$

Pseudo-reference

Pseudo-references are generally constructed with a metal wire directly immersed in the studied salt. Generally, an oxide is formed on the surface. Then, it is possible to use the metal and its oxide as a redox system which fixes the potential inside the salt. But, some problems can be observed, as an evolution of the potential with time or a dissolution of the metal electrode which conducts to salt pollution. Experiments have been conducted in order to determine if nickel, tungsten or carbon could be used as pseudo-reference.

Tungsten – Thermodynamic calculations have shown the instability of W in carbonate salt and its chemical oxidation to Na₂WO₄. That is confirmed by experiments which lead to the metal corrosion after immersion of W in carbonate salt: the weight loss of a tungsten wire immersed during one day in the salt is 0.2%.

Carbone – Experiments conducted with carbon as pseudo-reference have permitted to obtain voltammograms but with poor quality.

Nickel – Thermodynamic calculations have shown that nickel is stable in the carbonate salt. However, in presence of O₂, nickel is oxidized into NiO. Study conducted in the ternary eutectic

molten salt has shown that a NiO thick layer is formed during the first seconds of immersion because of O₂ oxidizing atmosphere [33]. In the (Li_{0.62}K_{0.38})₂CO₃ salt between 650°C and 750°C, the nickel oxide NiO has been observed under CO₂ [34]. Under Ar atmosphere, carbonate dissociation leads to CO₂ formation able to oxidize nickel. After nickel oxidation to NiO, Malinowska *et al.* [33] have explained that lithium is integrated into the NiO crystalline lattice. Sodium and potassium can also integrate the NiO crystalline lattice but lithium has been proven to be the most incorporated element [35]. When lithium incorporation is completed, electrochemical measurements conducted on nickel electrode lead to a stable OCP [33]. This result proves that Ni wire could be used as a pseudo-reference. From thermodynamic point of view, it is assumed that the redox system NiO/Ni is stable in the salt but its potential depends on a(Li₂O) (21) and thus on the atmosphere nature. This can present a drawback for the comparison of the potentials measured in different experimental conditions.

$$E_{NiO/Ni} = E_{NiO/Ni}^0 + \frac{2.3RT}{2F} \log \left(\frac{a_{NiO} \times a_{Li}^2}{a_{Ni} \times a_{Li_2O}} \right) + E_{Li^+/Li} \quad (21)$$

Internal reference electrode

In the case of an internal reference electrode, the potential is measured against the potential of a redox couple observed in the medium. The potential of this system has to be independent on the experimental conditions, such as the oxide activity or the nature of the atmosphere.

The cyclic voltammograms have been recorded in the Li₂CO₃-Na₂CO₃-K₂CO₃ at 600°C, at a gold working electrode.

Figure 6 shows a redox system before the cathodic limit (close to -1.25 V and -1.4 V/(Ni^{II}/Ni) depending on the gas atmosphere) with an angular point. The shape of these curves is typical of a solid compound formation and the redox system was attributed to the formation of gold-alkali metal alloy followed by its oxidation during the reverse scan. We observe a peak followed by a wave before the cathodic limit. The limitation of the current in this potential range is attributed to a diffusion process in the working electrode. Qiao *et al.* [36] have observed the same redox system in the LiF-NaF-KF molten salt and have attributed it to the Na⁺/Au₂Na redox couple by XRD characterisation of the electrode after electrolysis. In this study, to determine the nature of the material formed on the gold surface during cathodic polarization, one-hour electrolysis on the gold working electrode at the reduction peak potential has been conducted under each working atmosphere. At the end of the electrolysis, the gold electrode has been cut and analysed by XRD (Figure 7). Three species are detected: Au, LiKCO₃ and Au₂Na alloy.

Data sheets come from the Crystallography Open Database [37]–[39]. The redox system

encountered near the cathodic limit has then been attributed to the redox system $\text{Na}^+/\text{Au}_2\text{Na}$. The half-reaction and the corresponding Nernst equation are given by relations (22) and (23) respectively.



$$E_{\text{Na}^+/\text{Au}_2\text{Na}} = E_{\text{Na}^+/\text{Au}_2\text{Na}}^0 + \frac{2.3RT}{nF} \log \frac{a_{\text{Au}}^2 \times a_{\text{Na}^+}}{a_{\text{Au}_2\text{Na}}} \quad (23)$$

The redox system $\text{Na}^+/\text{Au}_2\text{Na}$ potential is independent of the Li_2O activity. It is then possible to use this redox couple as an internal reference. In Figure 8, the potential scale of the voltammograms is given against the internal reference electrode.

3.3 Electrochemical behaviour of the $\text{Li}_2\text{CO}_3\text{-Na}_2\text{CO}_3\text{-K}_2\text{CO}_3$ salt

Electroactivity domain – The electrochemical behaviour of the alkali carbonates salt has then been studied by voltammetry using a gold wire working electrode, a platinum wire counter electrode and a Ni wire pseudo-reference electrode, at 873 K under three working atmospheres. The potential scale of the voltammograms have been recalculated against the internal reference electrode $\text{Na}^+/\text{Au}_2\text{Na}$, this redox system being observed just before the cathodic limit. Figure 8 shows that the electroactivity domain depends on the atmosphere composition in equilibrium with the salt: 2.21 V under N_2/O_2 and Ar atmospheres, and 2.48 V under CO_2 atmosphere.

The thermodynamic calculations show that the salt electroactivity domain corresponds to the carbonate decomposition to O_2 (anodic limit) and C (cathodic limit) and is equal to 1.280 V under N_2/O_2 and Ar atmospheres, and 1.025 V under CO_2 atmosphere. The electroactivity domain experimentally measured is larger than the one calculated. That is generally due to activity coefficients lower than 1. Moreover, in contrast to thermodynamic calculations, the experimental electroactivity domain is larger under CO_2 than under O_2/N_2 and Ar atmosphere. That can be the consequence of irreversible charge transfer reactions or because the reactions characterizing the electroactivity range are not those foreseen by the thermodynamic calculations.

Characterization of the anodic limit – Many previous works have established that anodic limit corresponds to the carbonate oxidation to dioxygen (as presented in relation (7)) in the ternary carbonate eutectic [12], [13], [15], [24], [25], [31], [40], [41]. However, according to thermodynamic calculations, carbonate ions could be oxidized to peroxide [12], [13].

Gas chromatographic analyses have then been conducted to determine the gas produced at potentials corresponding to the anodic limit. The ternary salt $\text{Li}_2\text{CO}_3\text{-Na}_2\text{CO}_3\text{-K}_2\text{CO}_3$ has been prepared in the electrochemical cell, as presented previously. Electrolyses have been performed

at an anodic applied current of 60 mA, 120 mA, 180 mA, 240 mA and 360 mA at gold electrode for 60 min. During the electrolyses, an Ar gas flow has been maintained at 167.4 mL.min⁻¹ in the cell and the gas has been analysed by the μ GC instrument, which has previously been calibrated to detect H₂, O₂, N₂, CO and CO₂. Figure 9 and Figure 10 present chromatograms obtained during these electrolyses.

With the module 1 of the μ GC instrument, the retention times for H₂, O₂, N₂ and CO are 41 s, 50 s, 60 s and 95 s respectively. Figure 9 shows the dihydrogen formation during the electrolyses. That is probably the consequence of a small amount of water or hydroxide species still inside the molten salt which is reduced to H₂ at the cathode during the electrolysis (see relations (24) and (25)).



Dioxygen and dinitrogen are also observed with the module 1, even when no current is applied. The dinitrogen concentration does not increase significantly and does not depend on the current applied during the electrolysis. Thus, the observation of O₂ and N₂ when no current is applied has been attributed to a small leakage in the particle filters of the μ GC assembly which is responsible of an air inlet in the module ([O₂] = 35 ppm and [N₂] = 116 ppm). When a current is applied, Figure 9 shows that the ratio O₂/N₂ increases significantly and confirms that the carbonate ions are oxidised into dioxygen (equation (12)). No carbon monoxide is detected during all the experiment.

With the module 2 (Figure 10), the retention time for O₂/N₂ (in this module, O₂ and N₂ are not separated), CO₂ and H₂O are 35 s, 41 s and 69 s respectively. When no current is applied, the peak N₂/O₂ characteristic of the air introduced through the leakage in the system is observed (Figure 10). A small concentration of CO₂ is also detected ([CO₂] = 143 ppm), which can be explained by the carbonate ions dissociation into carbon dioxide and oxide ions (equation (1)). During each electrolysis, Figure 10 shows that the CO₂ concentration increases significantly. At the retention time of 69 s, H₂O is detected. This can be explained by the guard cell filled with water at the end of the reactor assembly (see Figure 1).

Figure 11 presents the variation of the O₂ and CO₂ concentrations measured by μ GC at the end of each electrolysis as a function of the current intensity. The results show that O₂ and CO₂ concentrations are proportional to the current of the electrolysis. The CO₂ and O₂ formation during the electrolysis confirm that carbonate ions are oxidised by the reaction (6). Considering this reaction, the ratio CO₂/O₂ should be equal to 2 while it is higher than 2.5 in all the

experiments. This could be explained by a second oxidation reaction which occurs on the gold electrode. As mentioned before, three compounds can be produced by carbonate ions oxidation: dioxygen (reaction (6)), super-oxide ions (reaction (7)) or peroxide ions (reaction (8)). Thermodynamic calculations show that carbonates ions oxidation to peroxide ions and to oxygen occur at closed potential values (equations (26) and (27) and Figure 2).



Same experiments have been conducted under CO₂ and O₂/N₂ (20%/80%) atmospheres (data not shown). The gas chromatographic analysis shows that under CO₂ atmosphere, the anodic limit corresponds to the carbonate oxidation to dioxygen. Under this atmosphere condition, it is not possible to quantify the amount of CO₂ produced during the electrolysis. The ratio [CO₂]/[O₂] has then not been determined. Under O₂/N₂ atmosphere, the O₂ concentration increases during the experiment and CO₂ has been detected. Thus, it appears that carbonate ions oxidation to dioxygen occurs for all the considered working atmospheres.

Characterization of the cathodic limit – Ingram *et al.* have shown thermodynamically and experimentally that the cathodic limit on platinum and gold electrodes is attributed to carbonate reduction to carbon [24], [31]. In this work, cathodic electrolyses have been performed on a platinum electrode and a solid deposit has been observed for each working atmosphere. These deposits, analysed by EDXS (energy-dispersive X-ray spectroscopy - Table 6), are mainly constituted of carbon which is in agreement with the previous studies [24], [31]. Only a few amounts of oxygen and potassium are detected which can be explained by the crystallization of carbonate salts on the electrode surface when it is taken out of the molten salt. This result agrees with the thermodynamic calculations presented previously even if the reaction occurs at a lower potential than expected by thermodynamic calculations. This is characteristic of an irreversible system.

On a gold electrode, the alloy Au₂Na formation has been observed at potentials just before the cathodic limit. When the applied potential during the electrolysis corresponds to the cathodic limit, a deposit has been observed and analysed by EDXS. In this case, the ratio [O]/[C] is around 3 and corresponds to carbonate salts deposition and not to carbon formation as previously observed on Pt electrode. This has also been observed when a very high reduction potential is applied on the gold electrode. Moreover, when the electrode is taken out of the salt,

sparks are observed which could be attributed to the oxidation by air of Na metal formed during the electrolysis. Therefore, at a gold electrode, the cathodic limit does not correspond to the reduction of carbonate ions to carbon but it seems to be attributed to the reduction of Na^+ to Na.

This is not in agreement with thermodynamic calculations presented previously nor the previous studies conducted by Ingram *et al.* [24], [31]. It seems that the carbonate ions reduction into carbon does not occur on the gold working electrode. The cathodic limit corresponds in this case to the reduction of Na^+ to Na which is preceded by the reduction of Na^+ to Au_2Na alloy with a limitation of the current by a diffusion process..

3.4 Carbonate decomposition

As explained previously, under argon atmosphere, carbonates are decomposed into carbon dioxide and oxide ions (relation (1)). To study this reaction, two methods are used: gas chromatography and TGA.

μGC analyses – Argon atmosphere is flowed through the cell from the beginning of the experiment, that is from the salt fusion. Chromatograms obtained proved the carbonate ions decomposition as CO_2 is detected. The GC analysis begins when the salt temperature is at 523 K. CO_2 formation has been followed by gases analysis. It allows the determination of the gas mole fraction (for example for CO_2 , x_{CO_2} , relation (28)). The amount of CO_2 formed as a function of time (the molar flow n_{CO_2}/t in mol%/min (relation (32)) is determined using ideal gas law (relations (29)) in which P is the pressure (101300 Pa), V the volume (m^3), R the ideal gas constant ($8.314 \text{ J}\cdot\text{mol}^{-1}\cdot\text{K}^{-1}$), n_t the total number of gas (mol) and T the temperature (K). The expression of volume is defined by the argon flow D (30) which is constant and equal to 167.4 mL/min.

$$x_{\text{CO}_2} = \frac{n_{\text{CO}_2}}{n_t} \quad (28)$$

$$PV = n_t RT \quad (29)$$

$$D = V/t \quad (30)$$

$$PDt = \frac{n_{\text{CO}_2}}{x_{\text{CO}_2}} RT \quad (31)$$

$$n_{\text{CO}_2}/t = x_{\text{CO}_2} \frac{PD}{RT} \quad (32)$$

Figure 12 presents the evolution of CO₂ molar flow as function of time (blue) and the evolution of temperature (red). During the first 4 hours of gases analysis, the temperature rises from 523 K to 873 K. During these first hours, the salt is not yet molten and the CO₂ molar flow variation presents two peaks which was attributed to two phenomena:

- At the lowest temperatures (from 0 h to 2 h): Water in the salt reacts with carbonates and forms carbonic acid (relation (33)). This acid is not stable and is decomposed to CO₂ and H₂O (relation (34)).



- At the highest temperatures (from 2 h to 4 h): a high release of CO₂ is observed when the salt starts to melt (reaction (2)).

After 4 hours, CO₂ molar flow becomes relatively constant and is equal to 0.02 ± 0.007 mmol.h⁻¹. From the molar flow, it is possible to determine the total quantity of CO₂ produced at a given time $n_{CO_2t_j}$ from relation (35) where $D_{CO_2t_i}$ is the CO₂ molar flow at the time t_i .

$$n_{CO_2t_j} = \sum_{i=m}^n (t_i - t_{i-1}) \times D_{CO_2t_i} \quad (35)$$

Figure 13 presents the evolution of the amount of CO₂ produced (blue) and the evolution of the salt temperature (red) with time. The increase of CO₂ is linear during the last 64 hours. According to the linear regression reported Figure 13, the amount of CO₂ can be estimated: after 68 hours, 1.49 mmol are formed. This should conduct to the formation of 1.49 mmol of Li₂O (Li₂O is more stable than Na₂O or K₂O). So, it corresponds to 14.9 mmol.kg⁻¹ of molten salt. Ge *et al.* have determined a solubility of Li₂O in the carbonate ternary eutectic of 5 mol% (457.8 mmol.kg⁻¹)[42]. So, all the Li₂O formed during the decomposition of the carbonates should be solubilized in the ternary studied molten salt.

Thermogravimetric analysis – A thermogravimetric analysis of the ternary carbonate salt has been performed under argon flow (60 mL.min⁻¹), to measure the weight loss of the salt. Figure 14 presents the temperature variation (red) and the weight loss measured (blue). It shows that during the first constant temperature stage at 573 K, the weight loss is equal to 1.07%. This can be attributed to the removal of moisture. During the temperature increase from 573 K to 873 K, the weight loss is 0.04%, and corresponds to the melting of the salt. Finally, a weight

loss of 0.38% is measured during the second constant temperature stage at 873 K. If this last loss is only attributed to the decomposition of the carbonates into O^{2-} and CO_2 , it would correspond to the formation of 0.1296 mmol of CO_2 .

Comparison of the TGA and μGC analysis – Table 7 compares the results obtained by gas chromatography (from 4 to 66.45 hours) and thermogravimetric analyses (from 10 to 80 hours). These results show that the carbonates decomposition per hour per exchange surface is approximately equal to 1×10^{-3} mmol.h⁻¹.cm⁻² for both techniques. The difference between the two values could be explained by the different gas flows for each study as it is higher for GC analysis than for TGA. This can lead to an increase of the carbonate decomposition kinetic.

4 Conclusion

The objectives of this work were to study the electrochemical behaviour of the Li_2CO_3 - Na_2CO_3 - K_2CO_3 (29.5/31.1/39.4 mol%) molten salt under three atmospheres (Ar, CO_2 and O_2/N_2) and its chemical degradation. The redox properties of several materials has also been considered to select the suitable electrodes for electrochemical measurements in the salt. The anodic and cathodic limits of the molten salt have been determined by thermodynamic calculation: the carbonate ions oxidation into dioxygen and their reduction into carbon respectively. The electrochemical domain width depends on lithium oxide activity: 1.280 V under Ar and O_2/N_2 atmospheres and 1.025 V under CO_2 .

According to the thermodynamic study of several materials in the considered carbonate molten salt, the electrodes have been defined for the electrochemical experiments: a Au working electrode, a Pt auxiliary electrode and a Ni pseudo-reference electrode. However, the experimental study by cyclic voltammetry has shown that the electrochemical reactions depend on pCO_2 and then on the nature and composition of atmosphere in equilibrium with the salt. This study has also put in evidence the redox system Na^+/Au_2Na , which can be used as an internal reference for the comparison of the potentials, since the potential of this redox couple is independent on the lithium oxide activity.

The electrochemical domain width measured by cyclic voltammetry is equal to 2.21 V under Ar and O_2/N_2 and 2.41 V under CO_2 . These values are higher than the ones calculated with the thermodynamic data and can be explained by activity coefficients lower than 1. The salt electrochemical behaviour has also been investigated by analysis of the gas formed during electrolyses at the anodic limit and by surface characterisation of the electrode after electrolyses at the cathodic limit. Gases analyses have shown that the anodic limit corresponds to the

carbonate ions oxidation into dioxygen, possibly peroxide ions and carbon dioxide. The cathodic limit corresponds to the carbonate ions reduction into carbon on platinum electrode which indicates that $\text{CO}_3^{2-}/\text{C}$ is an irreversible system.

The decomposition of the carbonate ions has been studied by GC and TGA and a rate of $1 \times 10^{-3} \text{ mmol.h}^{-1}.\text{cm}^{-2}$ has been measured by both techniques when the salt is under inert gas. A stabilization of the CO_2 pressure is observed after the melting of the salt.

Authors information

Corresponding authors:

sylvie.delpech@ijclab.in2p3.fr / 33 1 69 15 73 44

hugo.sauzet@ijclab.in2p3.fr

IJCLab, Université Paris-Saclay, CNRS/IN2P3, 15 rue Georges Clémenceau, 91405 Orsay cedex, France

IREIS, HEF Groupe, ZI Sud – 69 Avenue Benoît Fourneyron, CS 42077-42162 Andrézieux-Bouthéon, France

References

- [1] M. H. Kim, H. Yoshitake, H. Yokokawa, N. Kamiya, K. Ota, Cobalt and cerium coated Ni powder as a new candidate cathode material for MCFC, *Electrochim. Acta* 51 (2006) 6145.
- [2] M. Cassir, S. J. McPhail, A. Moreno, Strategies and new developments in the field of molten carbonates and high-temperature fuel cells in the carbon cycle, *Int. J. Hydrog. Energy*, 37 (2012) 19345.
- [3] A. Meléndez-Ceballos, V. Albin, V. Lair, A. Ringuedé, M. Cassir, A kinetic approach on the effect of Cs addition on oxygen reduction for MCFC application, *Electrochim. Acta* 184 (2015) 295.
- [4] T. Nejat Veziroglu, S. A. Sherif, F. Barbir, Chapter 7 - Hydrogen Energy Solutions, in *Environmental Solutions*, F. J. Agardy et N. L. Nemerow, Éd. Burlington: Academic Press, 2005, p. 143-180.
- [5] K. Sugiura, K. Takei, K. Tanimoto, Y. Miyazaki, The carbon dioxide concentrator by using MCFC, *J. Power Sources*, 118 (2003) 218.
- [6] L. Zhang, X. Huang, C. Qin, K. Brinkman., Y. Gong, S. Wang, K. Huang, First spectroscopic identification of pyrocarbonate for high CO_2 flux membranes containing highly interconnected three dimensional ionic channels, *Phys. Chem. Chem. Phys.*, 15, (2013), 13147.
- [7] E. Desmaele, Propriétés physico-chimiques des carbonates fondus par simulations atomistiques, Doctorate thesis, Université Pierre et Marie Curie - Paris VI, 2017.

- [8] D. Chery, Approche prévisionnelle de la valorisation électrochimique du CO₂ dans les carbonates fondus, Doctorate thesis, Université Paris 6, Paris, 2015.
- [9] K. Yasuda, F. Nozaki, R. Uehata, R. Hagiwara, Oxidative Dissolution of Tungsten Metal in Na₂CO₃ under Ar–O₂–CO₂ Atmosphere, *J. Electrochem. Soc.*, 167 (2020) 131501.
- [10] B. K. Andersen, Thermodynamic Properties of Molten Alkali Carbonates, Doctorate thesis, The Technical University of Denmark, Lyngby, 1975.
- [11] B. K. Andersen, Thermodynamic Properties of the O₂ - O₂⁻ - O₂²⁻ - O²⁻ system in molten alkali carbonates, *Acta Chem. Scand.*, 31 (1977) 242.
- [12] G. Moutiers, Propriétés électrochimiques dans les carbonates alcalins fondus a 500-850°C, Doctorate thesis, Université Paris 6, 1992.
- [13] M. Cassir, G. Moutiers, J. Devynck, Stability and Characterization of Oxygen Species in Alkali Molten Carbonate: A Thermodynamic and Electrochemical Approach, *J. Electrochem. Soc.*, 140 (1993) 3114.
- [14] B. Trémillon, Réactions dans les sels fondus, in *Électrochimie analytique et réactions en solution*, vol. Tome 1, Masson, 1993, p. 324.
- [15] G. J. Janz, Molten Carbonate Electrolytes as Acid-Base Solvent Systems, *J. Chem. Educ.*, 44 (1967) 581.
- [16] Y. Ito, K. Tsuru, J. Oishi, Y. Miyazaki, T. Kodama, Determination of the dissociation constant of molten Li₂CO₃/Na₂CO₃/K₂CO₃ using a stabilized zirconia oxide-ion indicator, *J. Power Sources*, 16 (1985) 75.
- [17] E. J. Mittemeijer, M. A. J. Somers, Thermochemical Surface Engineering of Steels. 2015.
- [18] C. F. Yeung, K. H. Lau, H. Y. Li, D. F. Luo, Advanced QPC complex salt bath heat treatment, *J. Mater. Process. Technol.*, 66 (1997) 249.
- [19] D. Pye, Practical nitriding and ferritic nitrocarburizing. ASM International, 2003.
- [20] B. Goh, F. Carotti, R. O. Scarlat, A Review of Electrochemical and Non-Electrochemical Approaches to Determining Oxide Concentration in Molten Fluoride Salts, *ECS Trans.*, 85 (2018) 1459.
- [21] S. Yoon, D. Kang, S. Sohn, J. Park, M. Lee, S. Choi, Reference Electrode at Molten Salt: A Comparative Analysis of Electroceramic Membranes, *J. Nucl. Fuel Cycle Waste Technol.*, 18 (2020) 143.
- [22] M. Pourbaix, Atlas d'équilibre électrochimiques. 1963.
- [23] R. Littlewood, Diagrammatic Representation of the Thermodynamics of Metal-Fused Chloride Systems, *J. Electrochem. Soc.*, 109 (1962) 525.
- [24] M. D. Ingram, G. J. Janz, The thermodynamics of corrosion in molten carbonates: Application of E/pCO₂ diagrams, *Electrochim. Acta*, 10 (1965) 783.
- [25] G. J. Janz, A. Conte, Potentiostatic polarization studies in fused carbonates—I. The noble metals, silver and nickel, *Electrochim. Acta*, 9 (1964) 1269.
- [26] B. Malinowska, M. Cassir, F. Delcorso, J. Devynck, Behaviour of nickel species in molten Li₂CO₃ + Na₂CO₃ + K₂CO₃ Part 1. Thermodynamic approach and electrochemical characterization under P(CO₂) = 1 atm, *J. Electroanal. Chem.*, 389 (1995) 21.
- [27] F. Lantelme, B. Kaplan, H. Groult, D. Devilliers, Mechanism for elemental carbon formation in molecular ionic liquids, *J. Mol. Liq.*, 83 (1999) 255.

- [28] M. Gao, B. Deng, Z. Chen, M. Tao, D. Wang, Enhanced kinetics of CO₂ electro-reduction on a hollow gas bubbling electrode in molten ternary carbonates, *Electrochem. Commun.*, 100 (2019) 81.
- [29] K. Le Van, H. Groult, F. Lantelme, M. Dubois, D. Avignant, A. Tressaud, S. Komaba, N. Kumagai, S. Sigrist, Electrochemical formation of carbon nano-powders with various porosities in molten alkali carbonates, *Electrochim. Acta*, 54 (2009) 4566.
- [30] G. Danner, M. Rey, Électrodes de référence pour hautes températures, *Electrochim. Acta*, 4 (1961) 274.
- [31] M. D. Ingram, B. Baron, G. J. Janz, The electrolytic deposition of carbon from fused carbonates, *Electrochim. Acta*, 11 (1966) 1629.
- [32] G. Duran-Klie, Étude du comportement de l'uranium et de l'iode dans le mélange de fluorures fondus LiF-ThF₄ à 650 °C, Doctorate thesis, Université Paris-Saclay, Orsay, 2017.
- [33] B. Malinowska, M. Cassir, J. Devynck, Behaviour of nickel species in molten Li₂CO₃ + Na₂CO₃ + K₂CO₃ Part 2. Electrochemical characterization under P(CO₂)=0.1 atm + P(O₂)=0.9 atm, P(Ar)=1 atm and P(O₂)=1 atm, *J. Electroanal. Chem.*, 417 (1996) 135.
- [34] T. Nishina, K. Takizawa, I. Uchida, Electrochemical characterization of in situ NiO formation in a molten carbonate, *J. Electroanal. Chem. Interfacial Electrochem.*, 263 (1989) 87.
- [35] B. Malinowska, M. Cassir, J. Devynck, Alkali insertion within NiO/Ni electrode in contact with molten Li₂CO₃-K₂CO₃ and Li₂CO₃-Na₂CO₃-K₂CO₃ at 650°C, *J. Power Sources*, 63 (1996) 27.
- [36] H. Qiao, T. Nohira, Y. Ito, Electrochemical formation of Au₂Na alloy and the characteristics of (Au₂Na/Au) reference electrode in a LiF/NaF/KF eutectic melt, *Electrochim. Acta*, 47 (2002) 4543.
- [37] F. P. Fehlner, S. M. Irving, Sodium-Gold Alloy Films, *J. Appl. Phys.*, 37 (1966) 3313.
- [38] E. R. Jette, F. Foote, Precision Determination of Lattice Constants, *J. Chem. Phys.*, 3 (1935) 605.
- [39] Y. Idemoto, J. W. Richardson, N. Koura, S. Kohara, C.-K. Loong, Crystal structure of (Li_xK_{1-x})₂CO₃ (x=0, 0.43, 0.5, 0.62, 1) by neutron powder diffraction analysis, *J. Phys. Chem. Solids*, 59 (1998) 14.
- [40] G. J. Janz, F. Saegusa, Anodic Polarization Curves in Molten Carbonate Electrolysis, *J. Electrochem. Soc.*, 108 (1961) 663.
- [41] G. J. Janz, Colom, Francisco, F. Saegusa, Oxygen Overpotential in Molten Carbonates, *J. Electrochem. Soc.* 107 (1960) 581.
- [42] J. Ge, L. Zhang, J. Lu, J. Zhu, S. Jiao, Solubility of Oxide Ion in Molten Chloride and Carbonate Containing Li, Na, K and/or Ca Added with Li₂O or CaO, *J. Electrochem. Soc.*, 163 (2016) E300-E304.

Table 1: Chemical composition of the studied molten salt.

	Li_2CO_3	Na_2CO_3	K_2CO_3
<i>Molar percentage</i>	29.5	31.1	39.4
<i>Mass percentage</i>	19.9	30.3	49.8

Table 2: Autodissociation constants K_{Ω} of each alkali carbonate at 873 K.

Li_2CO_3	Na_2CO_3	K_2CO_3
4.56×10^{-6}	1.82×10^{-12}	1.45×10^{-16}

Table 3: Salt oxoacidity limits.

	Oxobasic limit	Oxoacidic limit
a_{Li_2O}	1	1.34x10 ⁻⁶
$pa_{Li_2O} = -\log(a_{Li_2O})$	0	5.87

Table 4: Salt redox systems and the associated $E = f(a_{Li_2O})$ relations

Redox couple	Reaction – Relation $E = f(a_{Li_2O})$
Li^+/Li $E_{Li^+/Li}^0 = 0 V$	$E_{Li^+/Li} = E_{Li^+/Li}^0 + \frac{2.3RT}{nF} \log \frac{a_{Li_2CO_3}}{a_{Li}^2 \times a_{CO_3^{2-}}}$
Na^+/Na $E_{Na^+/Na}^0 = 0.42 V$	$Li_2CO_3 + 2Na \rightarrow 2Li + Na_2CO_3$ $E_{Na^+/Na} = E_{Na^+/Na}^0 + 2,3 \frac{RT}{2F} \log \left(\frac{a_{Na_2CO_3} \times a_{Li}^2}{a_{Na}^2 \times a_{Li_2CO_3}} \right) + E_{Li^+/Li}$
K^+/K $E_{K^+/K}^0 = 0.35 V$	$Li_2CO_3 + 2K \rightarrow 2Li + K_2CO_3$ $E_{K^+/K} = E_{K^+/K}^0 + 2,3 \frac{RT}{2F} \log \left(\frac{a_{K_2CO_3} \times a_{Li}^2}{a_K^2 \times a_{Li_2CO_3}} \right) + E_{Li^+/Li}$
$CO_3^{2-}/CO(g)$ $E_{CO_3^{2-}/CO}^0 = 0.97 V$	$CO(g) + 2Li_2O \rightarrow 2Li + Li_2CO_3$ $E_{CO_3^{2-}/CO} = E_{CO_3^{2-}/CO}^0 + \frac{2.3RT}{2F} \log \left(\frac{a_{Li_2CO_3} \times a_{Li}^2}{a_{CO} \times a_{Li_2O}^2} \right) + E_{Li^+/Li}$
CO_3^{2-}/C $E_{CO_3^{2-}/C}^0 = 1.24 V$	$C + 3Li_2O \rightarrow 4Li + Li_2CO_3$ $E_{CO_3^{2-}/C} = E_{CO_3^{2-}/C}^0 + \frac{2.3RT}{4F} \log \left(\frac{a_{Li_2CO_3} \times a_{Li}^4}{a_C \times a_{Li_2O}^3} \right) + E_{Li^+/Li}$
$O_2(g)/CO_3^{2-}$ $E_{O_2/CO_3^{2-}}^0 = 2.96 V$	$Li_2CO_3 \rightarrow 2Li + CO_2(g) + \frac{1}{2}O_2(g)$ $E_{O_2/CO_3^{2-}} = E_{O_2/CO_3^{2-}}^0 + 2,3 \frac{RT}{2F} \log \left(\frac{a_{O_2}^{0.5} \times K_{\Omega} \times a_{Li}^2}{a_{Li_2O}} \right) + E_{Li^+/Li}$
O_2^-/CO_3^{2-} $E_{O_2^-/CO_3^{2-}}^0 = 3.27 V$	$K_2CO_3 + 3Li_2CO_3 \rightarrow 6Li + 4CO_2(g) + 2KO_2$ $E_{O_2^-/CO_3^{2-}} = E_{O_2^-/CO_3^{2-}}^0 + 2,3 \frac{RT}{6F} \log \left(\frac{a_{Li}^6 \times a_{KO_2}^2 \times K_{\Omega}^4 \times a_{Li_2CO_3}}{a_{K_2CO_3} \times a_{Li_2O}^4} \right) + E_{Li^+/Li}$
O_2^{2-}/CO_3^{2-} $E_{O_2^{2-}/CO_3^{2-}}^0 = 3.62 V$	$2Li_2CO_3 \rightarrow 2Li + 2CO_2(g) + Li_2O_2$ $E_{O_2^{2-}/CO_3^{2-}} = E_{O_2^{2-}/CO_3^{2-}}^0 + 2,3 \frac{RT}{6F} \log \left(\frac{K_{\Omega}^2 \times a_{Li}^2 \times a_{Li_2O_2}}{a_{Li_2O}^2} \right) + E_{Li^+/Li}$

With $a_{M_2CO_3} = x_{M_2CO_3}$ ($x_{M_2CO_3}$ the molar fraction of compound M_2CO_3 , $M = Li, Na$ or K), $a_M = 1$, $a_{CO} = 1$, $a_C = 1$, $a_{CO_3^{2-}} = 1$, $a_{O_2} = 1$ or 10^{-3} , $a_{KO_2} = 1$ or 10^{-3} , $a_{Li_2O_2} = 1$ and $a_{Li_2O} \in [1.34 \times 10^{-6}; 1]$

Table 5: Materials of interest redox couple and their relation $E = f(a_{Li_2O})$ presented

Figure 3 and Figure 4.

Redox couple	Reaction – Relation $E = f(a_{Li_2O})$
Li^+/Li $E_{Li^+/Li}^0 = 0 V$	$E_{Li^+/Li} = E_{Li^+/Li}^0 + \frac{2.3RT}{nF} \log \frac{a_{Li_2CO_3}}{a_{Li}^2 \times a_{CO_3^{2-}}}$
Au_2O_3/Au $E_{Au_2O_3/Au}^0 = 2.89 V$	$2Au + 3Li_2O \rightarrow Au_2O_3 + 6Li$ $E_{Au_2O_3/Au} = E_{Au_2O_3/Au}^0 + \frac{2.3RT}{6F} \log \left(\frac{a_{Au_2O_3} \times a_{Li}^6}{a_{Au}^2 \times a_{Li_2O}^3} \right) + E_{Li^+/Li}$
PtO/Pt $E_{PtO/Pt}^0 = 2.51 V$	$Pt + Li_2O \rightarrow PtO + 2Li$ $E_{PtO/Pt} = E_{PtO/Pt}^0 + \frac{2.3RT}{2F} \log \left(\frac{a_{PtO} \times a_{Li}^2}{a_{Pt} \times a_{Li_2O}} \right) + E_{Li^+/Li}$
PtO_2/PtO $E_{PtO_2/PtO}^0 = 2.54 V$	$PtO + Li_2O \rightarrow PtO_2 + 2Li$ $E_{PtO_2/PtO} = E_{PtO_2/PtO}^0 + \frac{2.3RT}{2F} \log \left(\frac{a_{PtO_2} \times a_{Li}^2}{a_{PtO} \times a_{Li_2O}} \right) + E_{Li^+/Li}$
NiO/Ni $E_{NiO/Ni}^0 = 1.67 V$	$Ni + Li_2O \rightarrow NiO + 2Li$ $E_{NiO/Ni} = E_{NiO/Ni}^0 + \frac{2.3RT}{2F} \log \left(\frac{a_{NiO} \times a_{Li}^2}{a_{Ni} \times a_{Li_2O}} \right) + E_{Li^+/Li}$
$NiCO_3/Ni$ $E_{NiCO_3/Ni}^0 = 2.55 V$	$Ni + Li_2CO_3 \rightarrow NiCO_3 + 2Li$ $E_{NiCO_3/Ni} = E_{NiCO_3/Ni}^0 + \frac{2.3RT}{2F} \log \left(\frac{a_{NiCO_3} \times a_{Li}^2}{a_{Ni} \times a_{Li_2CO_3}} \right) + E_{Li^+/Li}$
Na_2WO_4/W $E_{Na_2WO_4/W}^0 = 1.11 V$	$W + 4Li_2O + Na_2CO_3 \rightarrow Na_2WO_4 + 6Li + Li_2CO_3$ $E_{Na_2WO_4/W} = E_{Na_2WO_4/W}^0 + \frac{2.3RT}{6F} \log \left(\frac{a_{Na_2WO_4} \times a_{Li}^6 \times a_{Li_2CO_3}}{a_W \times a_{Li_2O}^6 \times a_{Na_2CO_3}} \right) + E_{Li^+/Li}$

With $a_{M_2CO_3} = x_{M_2CO_3}$ ($x_{XM_2CO_3}$ the M_2CO_3 molar fraction and $M = Li, Na, K$), $a_X = 1$ (with $X = Li, Na, K, Au, Pt, Ni, W$), $a_{X_xO_y} = 1$ (with $X = Au, Pt, Ni, W$), $a_{NiCO_3} = 0.001$, $a_{CO_3^{2-}} = 1$, and $a_{Li_2O} \in [1.34 \times 10^{-6}; 1]$

Table 6: Chemical composition determined by EDXS of the deposits obtained on Au and Pt electrodes in Li₂CO₃-Na₂CO₃-K₂CO₃ melt at 873 K after cathodic electrolysis.

Electrode – atmosphere	C (%at.)	O (%at.)	K (%at.)	Na (%at.)	[O]/[C]
Pt – N₂/O₂	91.7	8.1	0.2	0	<0.1
Pt – Ar	91.8	7.2	0.7	0	<0.1
Pt – CO₂	92.9	6.5	0.4	0	<0.1
Au – Ar	22.9	59.7	0.6	16.8	2.6

Table 7: Comparison between TGA and μ GC results for the analysis of the carbonates decomposition into CO_2 .

	μ GC	TGA	Ratio TGA/ μ GC
Salt quantity (g)	100.826	1.500953	/
Debit ($\text{mL}\cdot\text{min}^{-1}$)	167.4	60	/
Exchange surface (cm^2)	20.43	2.01	/
CO_2 quantity detected (mmol)	1.33	0.13	/
Time of the study (h)	62.45	70	/
CO_2 quantity detected per hour per quantity of salt ($\text{mmol}\cdot\text{h}^{-1}\cdot\text{g}^{-1}$)	2.1×10^{-4}	1.2×10^{-3}	5.9
Exchange surface/Salt quantity ($\text{cm}^2\cdot\text{g}^{-1}$)	0.2	1.3	6.6
CO_2 quantity detected per hour per exchange surface ($\text{mmol}\cdot\text{h}^{-1}\cdot\text{cm}^{-2}$)	1.0×10^{-3}	9.2×10^{-4}	0.9

Figure 1: Experimental set-up used for the electrochemical measurements and μ GC analysis.

(1) and (2) electrochemical cell, (3) Alumina crucible, (4) reference electrode (5) pseudo-reference, (6) and (7) metals used as working and auxiliary electrodes, (8) and (9) empty guard cells to prevent water to go inside μ GC instrument or in the salt, (10) guard cell fill of water and (11) guard cell fill with active carbon.

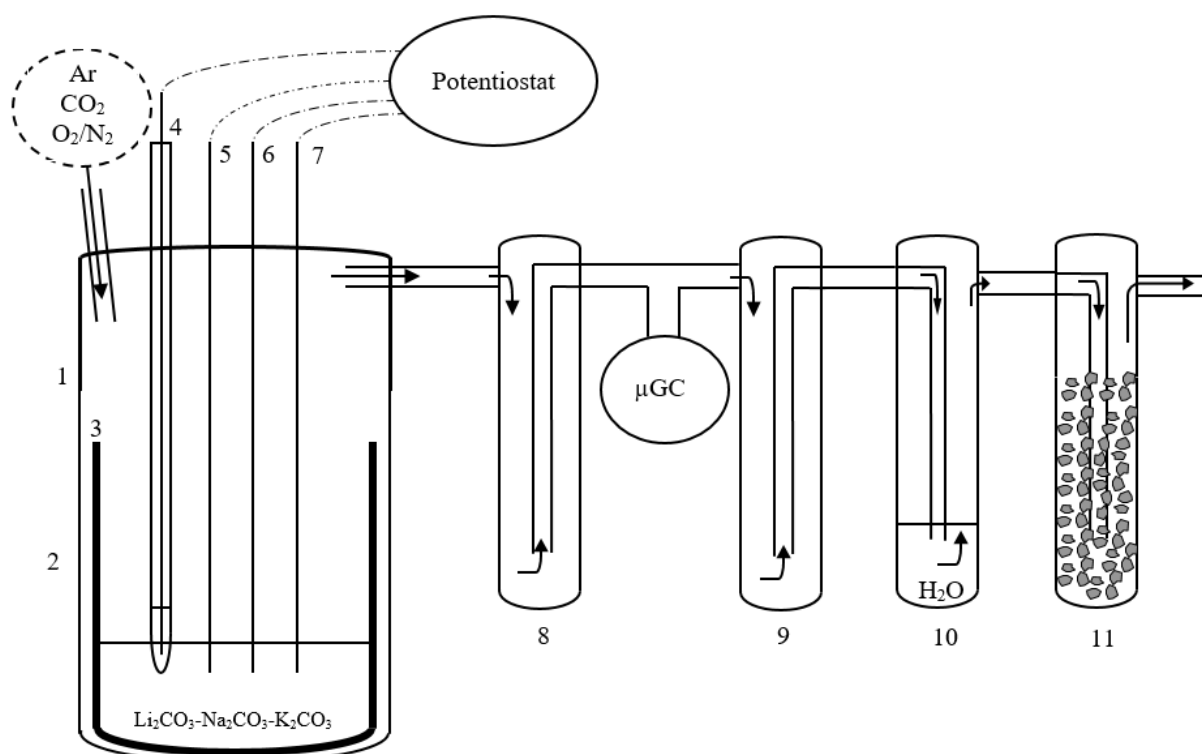


Figure 2: Potential-acidity diagram of the molten salt $\text{Li}_2\text{CO}_3 - \text{Na}_2\text{CO}_3 - \text{K}_2\text{CO}_3$ (29.5 - 31.1 - 39.4 mol%) at 873 K calculated with the HSC Database **a) with $a(\text{O}_2^{2-}) = a(\text{O}_2^-) = 1$ and b) with $a(\text{O}_2^{2-}) = a(\text{O}_2^-) = 10^{-3}$.**

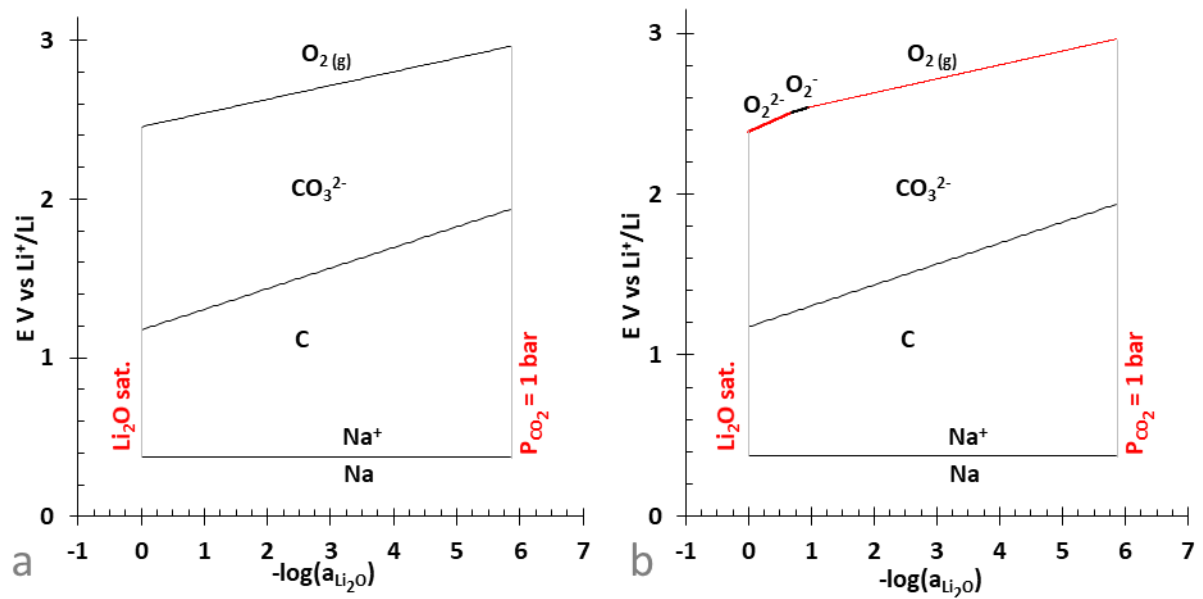


Figure 3: Potential-acidity diagrams of Gold (left) and Platinum (right) in molten carbonate at 873 K calculated with HSC database. α , β and γ lines correspond to CO_3^{2-} oxidation into O_2 , CO_3^{2-} reduction into C and Na^+ reduction into Na respectively.

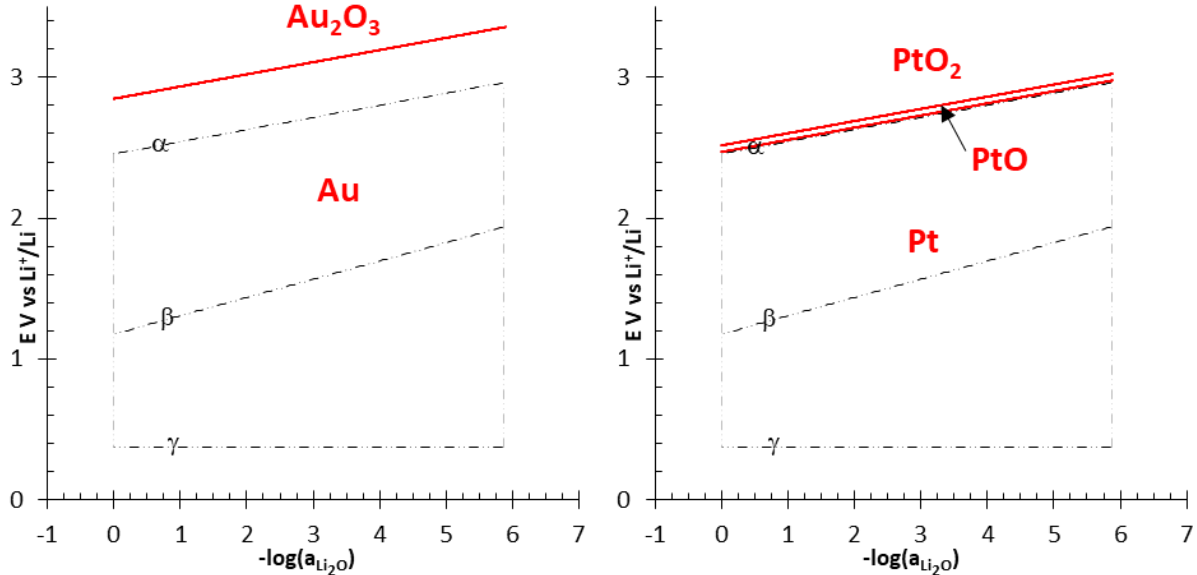


Figure 4: Nickel (left) and Tungsten (right) stability potential in function of oxoacidity in molten carbonate at 873 K calculated with the HCS database. α , β and γ lines correspond to CO_3^{2-} oxidation into O_2 , CO_3^{2-} reduction into C and Na^+ reduction into Na respectively.

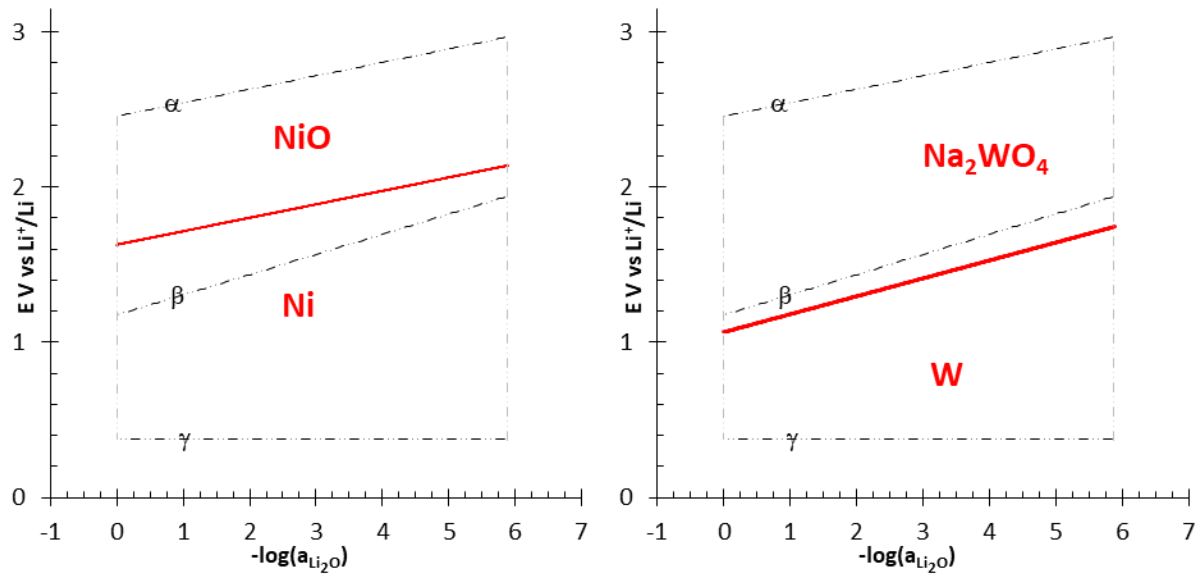


Figure 5 : Reference electrodes used in the references [12], [30], [32] and tested in this study.

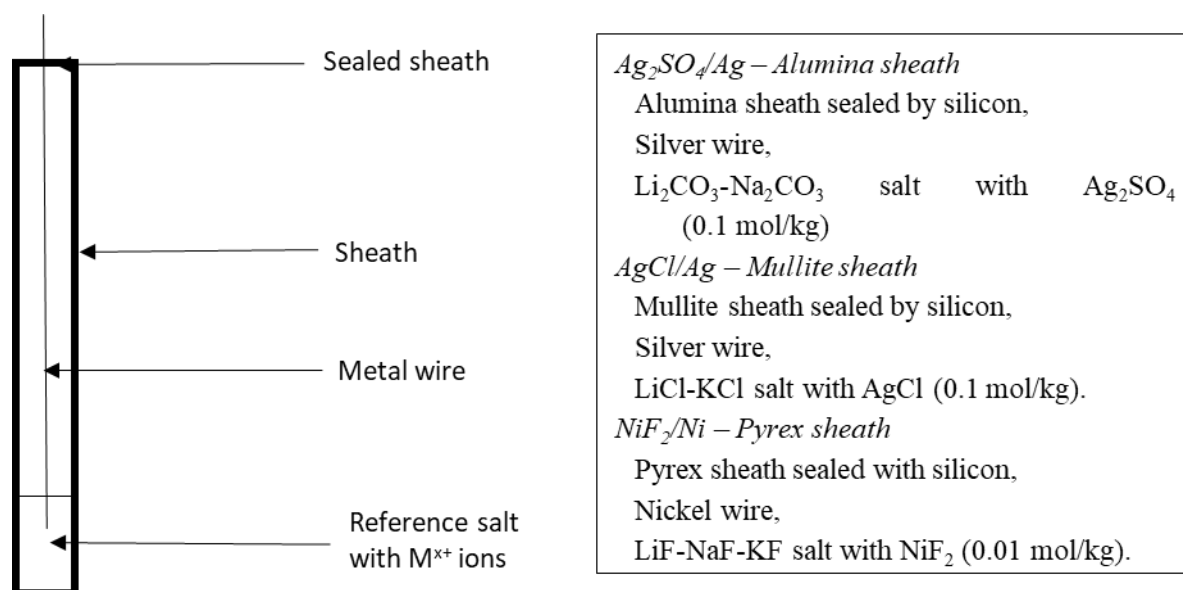


Figure 6: Cyclic voltammograms obtained on Au electrode in $\text{Li}_2\text{CO}_3\text{-Na}_2\text{CO}_3\text{-K}_2\text{CO}_3$ melt at 873 K with a scan rate of $100 \text{ mV}\cdot\text{s}^{-1}$ under CO_2 , O_2/N_2 and Ar atmosphere. The reference electrode is a Ni wire immersed in a Pyrex sheath containing a NiF_2 ($10^{-2} \text{ mol}\cdot\text{kg}^{-1}$) solution in LiF-NaF-KF .

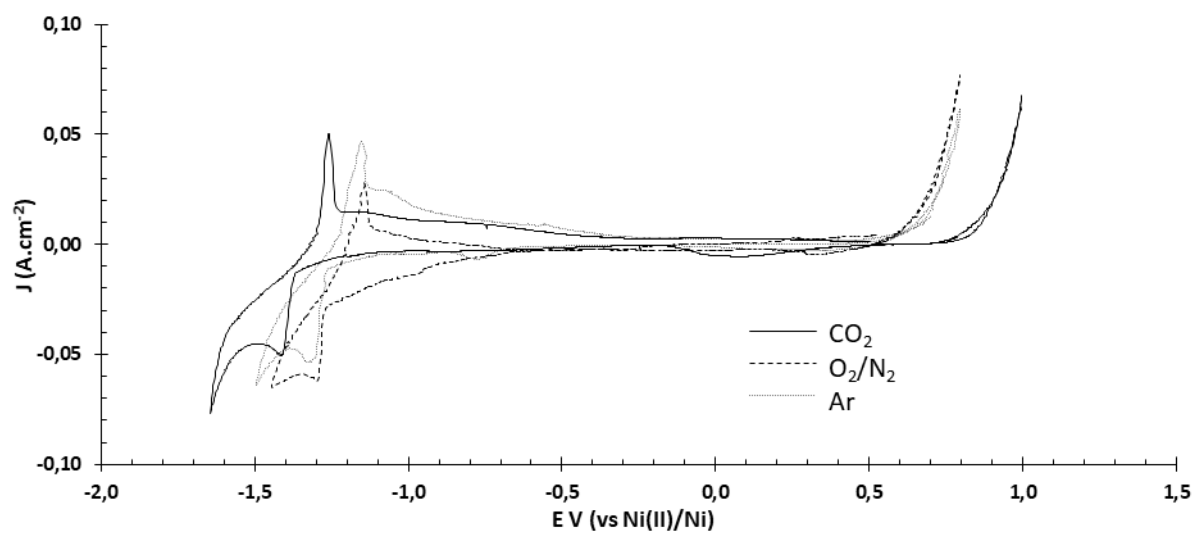


Figure 7: Gold electrode surface X-ray diffractogram after one hour-electrolysis at the reduction potential of the peak near the cathodic limit in $\text{Li}_2\text{CO}_3\text{-Na}_2\text{CO}_3\text{-K}_2\text{CO}_3$ melt at 873 K under Ar. Data sheets[37]–[39] come from the Crystallography Open Database. Au_2Na : cubic cell unit, $a=0.785$ nm.

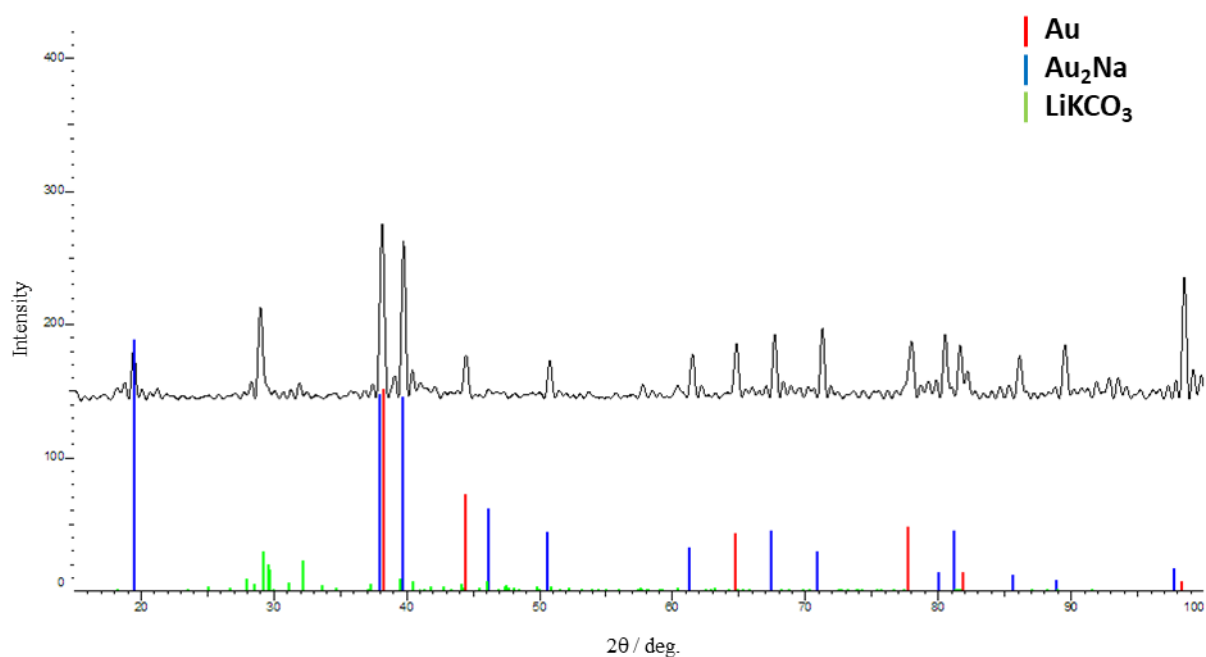


Figure 8: Cyclic voltammograms recorded at Au electrode in $\text{Li}_2\text{CO}_3\text{-Na}_2\text{CO}_3\text{-K}_2\text{CO}_3$ melt at 873 K with a scan rate of $100 \text{ mV}\cdot\text{s}^{-1}$ under CO_2 , O_2/N_2 and Ar atmosphere. The potential is measured against the internal reference $\text{Na}^+/\text{Au}_2\text{Na}$.

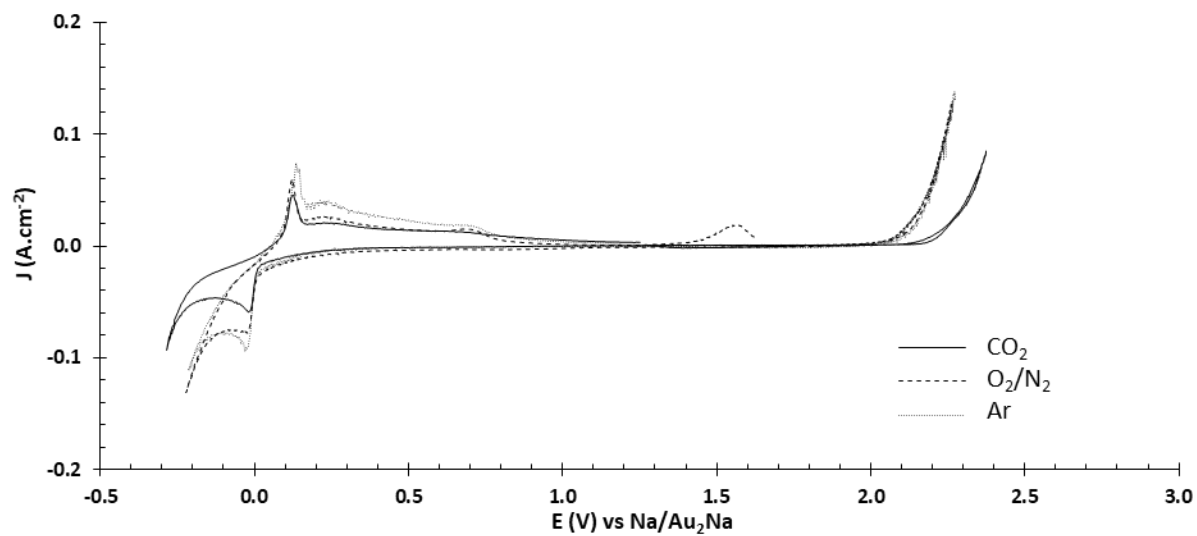


Figure 9: Gas chromatograms obtained on module 1 at the end of electrolyses performed by applying an anodic current in $\text{Li}_2\text{CO}_3\text{-Na}_2\text{CO}_3\text{-K}_2\text{CO}_3$ melt at 873 K under Ar atmosphere for 60 min.

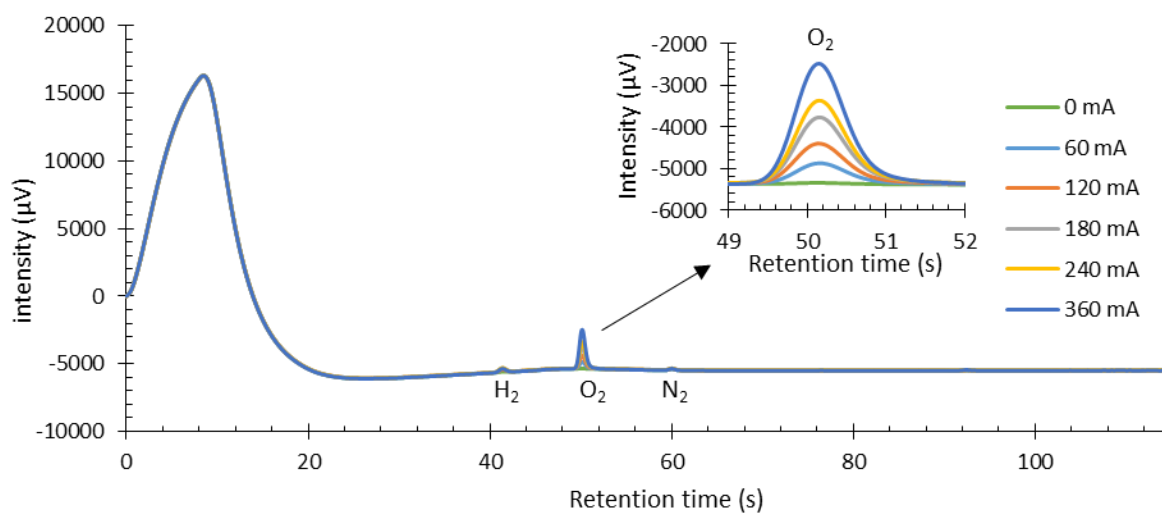


Figure 10: Gas chromatograms obtained on module 2 at the end electrolyses performed by applying an anodic current in $\text{Li}_2\text{CO}_3\text{-Na}_2\text{CO}_3\text{-K}_2\text{CO}_3$ melt at 873 K under Ar atmosphere for 60 min.

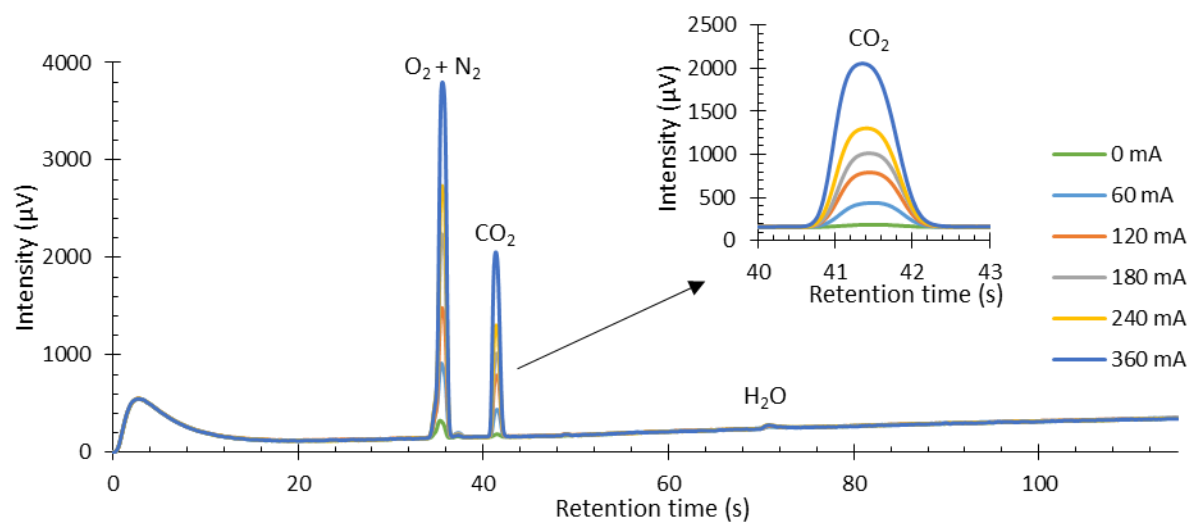


Figure 11: O₂ and CO₂ concentration after electrolyses of 60 min on the anodic limit in function of current intensity in Li₂CO₃-Na₂CO₃-K₂CO₃ melt at 873 K under Ar atmosphere.

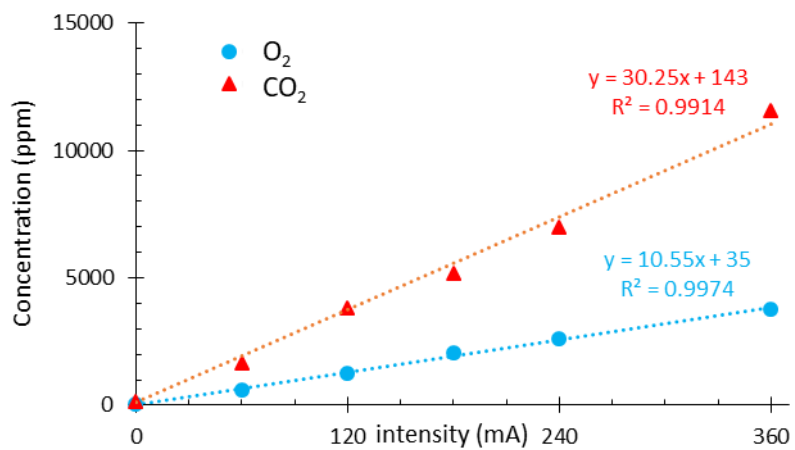


Figure 12: molar flow of CO₂ produced by the decomposition of the salt Li₂CO₃-Na₂CO₃-K₂CO₃ molten at 873 K under Ar.

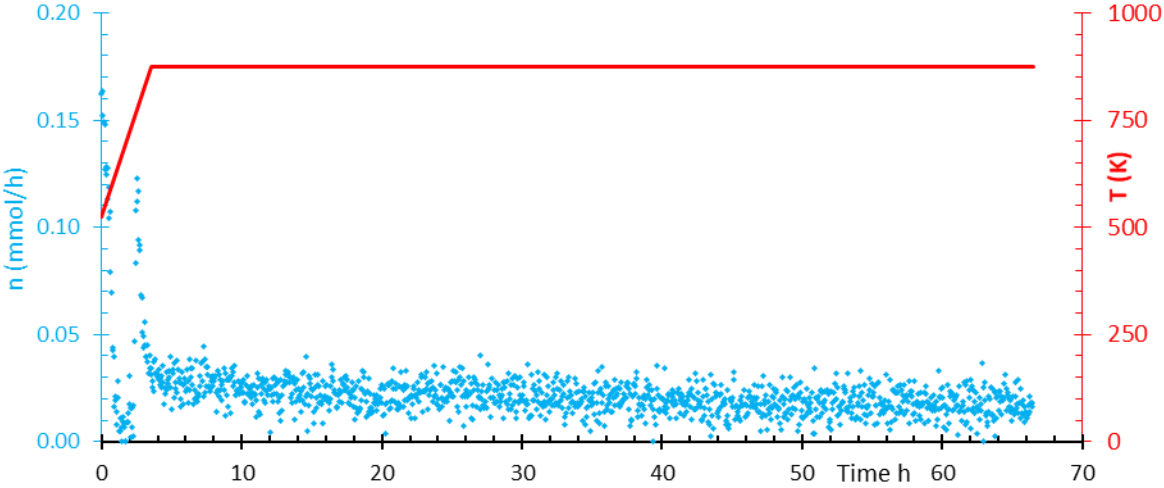


Figure 13: CO₂ molar amount formed by the decomposition of the salt Li₂CO₃-Na₂CO₃-K₂CO₃ molten at 873 K under Ar.

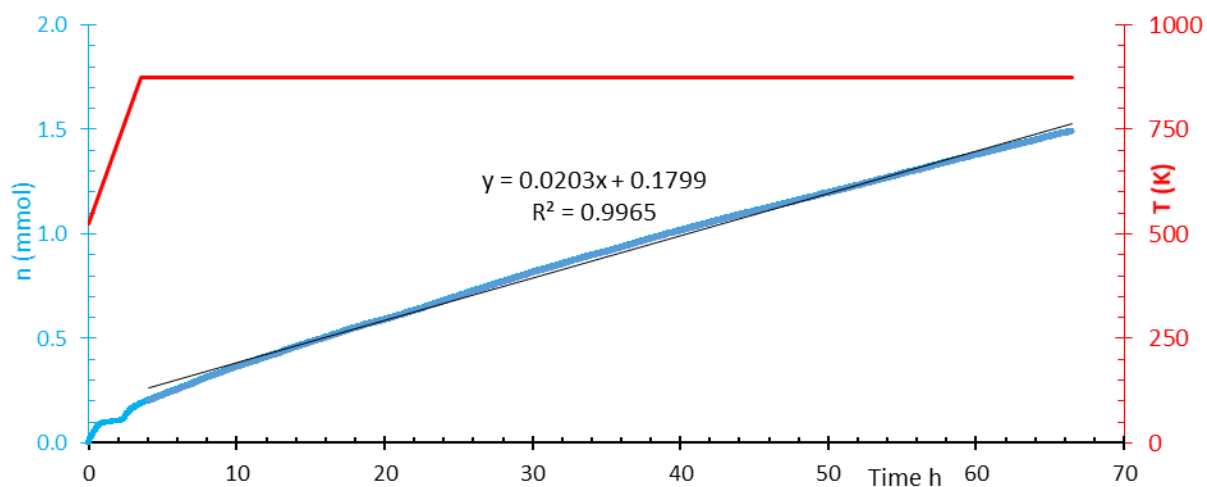


Figure 14: TGA performed on 1500.953 mg of $\text{Li}_2\text{CO}_3\text{-Na}_2\text{CO}_3\text{-K}_2\text{CO}_3$ molten under Ar.

